The Astrophysical Journal, 756:63 (10pp), 2012 September 1 doi:10.1088/0004-637X/756/1/63

THE AFTERGLOW AND ENVIRONMENT OF THE SHORT GRB 111117A

R. Margutti[1], E. Berger[1], W. Fong[1], B. A. Zauderer[1], S. B. Cenko[2], J. Greiner[3], A. M. Soderberg[1], A. Cucchiara[4], A. Rossi[5], S. Klose[5], S. Schmidl[5], D. Milisavljevic[1], and N. Sanders[1]
[1] Harvard-Smithsonian Center for Astrophysics, 60 Garden Street, Cambridge, MA 02138, USA
[2] Department of Astronomy, University of California, Berkeley, CA 94720, USA
[3] Max-Planck-Institut für Extraterrestrische Physik, D-85740 Garching, Germany
[4] Department of Astronomy and Astrophysics, UCO/Lick Observatory, University of California, 1156 High Street, Santa Cruz, CA 95064, USA
[5] Thüringer Landessternwarte Tautenburg, Sternwarte 5, D-07778 Tautenburg, Germany
Received 2012 May 31; accepted 2012 July 2; published 2012 August 16

ABSTRACT

We present multi-wavelength observations of the afterglow of the short GRB 111117A, and follow-up observations of its host galaxy. From rapid optical and radio observations, we place limits of $r \gtrsim 25.5$ mag at $\delta t \approx 0.55$ days and $F_\nu(5.8\,\mathrm{GHz}) \lesssim 18$ μJy at $\delta t \approx 0.50$ days, respectively. However, using a *Chandra* observation at $\delta t \approx 3.0$ days we locate the absolute position of the X-ray afterglow to an accuracy of $0\farcs22$ (1σ), a factor of about six times better than the *Swift*/XRT position. This allows us to robustly identify the host galaxy and to locate the burst at a projected offset of $1\farcs25 \pm 0\farcs20$ from the host centroid. Using optical and near-IR observations of the host galaxy we determine a photometric redshift of $z = 1.3^{+0.3}_{-0.2}$, one of the highest for any short gamma-ray burst (GRB), leading to a projected physical offset for the burst of 10.5 ± 1.7 kpc, typical of previous short GRBs. At this redshift, the isotropic γ-ray energy is $E_{\gamma,\mathrm{iso}} \approx 3.0 \times 10^{51}$ erg (rest-frame 23–2300 keV) with a peak energy of $E_{\mathrm{pk}} \approx 850$–2300 keV (rest-frame). In conjunction with the isotropic X-ray energy, GRB 111117A appears to follow our recently reported $E_{\mathrm{x,iso}}$–$E_{\gamma,\mathrm{iso}}$–E_{pk} universal scaling. Using the X-ray data along with the optical and radio non-detections, we find that for a blastwave kinetic energy of $E_{\mathrm{K,iso}} \approx E_{\gamma,\mathrm{iso}}$ erg, the circumburst density is $n_0 \approx 3 \times 10^{-4} - 1\ \mathrm{cm}^{-3}$ (for a range of $\epsilon_B = 0.001$–0.1). Similarly, from the non-detection of a break in the X-ray light curve at $\delta t \lesssim 3$ days, we infer a minimum opening angle for the outflow of $\theta_j \gtrsim 3$–10° (depending on the circumburst density). We conclude that *Chandra* observations of short GRBs are effective at determining precise positions and robust host galaxy associations in the absence of optical and radio detections.

Key word: gamma-ray burst: individual (GRB111117A)

Online-only material: color figures

1. INTRODUCTION

Precise localizations of short-duration gamma-ray bursts (GRBs) are critical for studies of their explosion properties, environments, and progenitors. In particular, such localizations can provide secure associations with host galaxies, and hence redshift and offset measurements (e.g., Berger et al. 2007; Fong et al. 2010; Berger 2011). To date, most subarcsecond positions for short GRBs have relied on the detection of optical afterglows (e.g., Berger et al. 2005; Hjorth et al. 2005; Soderberg et al. 2006). However, X-ray emission is detected from a larger fraction of short bursts, and therefore observations with the *Chandra X-ray Observatory* can equally provide precise positions even in the absence of optical detections. Indeed, *Chandra* detections have been previously made for short GRBs 050709, 050724, 051221A, 080503, and 111020A (Fox et al. 2005; Berger et al. 2005; Burrows et al. 2006; Grupe et al. 2006; Soderberg et al. 2006; Perley et al. 2009; Fong et al. 2012), but only in the latter case *Chandra* provided the sole route to a precise position (Fong et al. 2012). In the other four cases, the afterglow was also detected in the optical, as well as in the radio for GRBs 050724 and 051221A (Berger et al. 2005; Soderberg et al. 2006).

The advantage of precise X-ray positions is that the X-ray flux is potentially independent of the circumburst density if the synchrotron cooling frequency is located redward of the X-ray band. Thus, X-ray detections can in principle reduce any bias for small offsets that may arise from optical detections, which do depend on the density (although, see Berger 2010 for short GRBs with optical afterglows and evidence for large offsets of ~50–100 kpc).

Here, we present a *Chandra* detection of the X-ray afterglow of short GRB 111117A at $\delta t \approx 3$ days, which leads to a robust association with a galaxy at a photometric redshift of $z \approx 1.3$ and to a precise offset measurement. Among short GRBs, only GRBs 050724 and 051221A were detected at later times in X-rays. Using the *Chandra* and *Swift*/XRT data we study the properties of the X-ray afterglow in the context of the short GRB sample, and in conjunction with deep optical and radio upper limits we place constraints on the circumburst density. Similarly, optical/near-IR observations of the host allow us to determine its physical properties (star formation rate, stellar mass, stellar population age).

Throughout the paper we use the convention $F_\nu(\nu, t) \propto \nu^\beta t^\alpha$, where the spectral energy index is related to the spectral photon index by $\Gamma = 1 - \beta$. All uncertainties are quoted at 68% confidence level, unless otherwise noted. Magnitudes are reported in the AB system and have been corrected for Galactic extinction (Schlafly & Finkbeiner 2011). Finally, we use the standard cosmological parameters: $H_0 = 71$ km s^{-1} Mpc^{-1}, $\Omega_\Lambda = 0.73$, and $\Omega_\mathrm{M} = 0.27$.

2. OBSERVATIONS AND ANALYSIS

GRB 111117A was detected on 2011 November 17.510 UT (Mangano et al. 2011a) by the Burst Alert Telescope (BAT; Barthelmy et al. 2005) on board the *Swift* satellite (Gehrels et al. 2004), with a ground-calculated positional accuracy of

1.′7 radius (90% containment; Sakamoto et al. 2011a). The burst was also detected by the *Fermi* Gamma-Ray Burst Monitor (GBM) in the energy range 10–1000 keV (Foley & Jenke 2011).

Follow-up observations with the X-Ray Telescope (XRT; Burrows et al. 2005) commenced at $\delta t \approx 80$ s and resulted in the detection of a fading X-ray source located at R.A. $= 00^{\rm h}50^{\rm m}46^{\rm s}.22$ and decl. $= +23^{\circ}00'39''.2$ (J2000), with an uncertainty of 2.″1 radius (90% containment; Melandri et al. 2011b). GRB111117A is therefore part of the handful of short GRBs promptly repointed by *Swift*/XRT and with broadband spectral coverage during the prompt emission. The UV–Optical Telescope (UVOT; Roming et al. 2005) began observations of the field at $\delta t \approx 137$ s but no corresponding source was found within the XRT position to limits of $\gtrsim$19.5–21.5 mag in the first 1300 s (Oates & Mangano 2011).

Ground-based optical observations commenced at $\delta t \approx 2$ hr with a non-detection at $R \approx 22.2$ mag (Zhao et al. 2011), and eventually led to the detection of an extended source with $r \approx 24$ mag, identified as the potential host galaxy of GRB 111117A (Andersen et al. 2011; Fong et al. 2011b; Cenko & Cucchiara 2011; Schmidl et al. 2011; Melandri et al. 2011a).

Finally, a *Chandra* observation at $\delta t \approx 3.0$ days led to the detection of the X-ray afterglow (Sakamoto et al. 2011b), and a refined analysis relative to our optical images from the Magellan 6.5 m telescope provided a correction to the native *Chandra* astrometry and an initial offset from the host galaxy of about 1″ (Berger et al. 2011). The analysis presented here supercedes the *Chandra* position quoted in the GCN circulars (Berger et al. 2011).

2.1. γ-Ray Observations

We processed the *Swift*/BAT data with the latest version of the HEASOFT package (v6.11), using the `batgrbproduct` script to generate event lists and quality maps for the 64 ms mask-weighted and background-subtracted light curves (Figure 1). The ground-refined coordinates provided by Sakamoto et al. (2011a) were adopted, and standard filtering and screening criteria were applied. We also used the mask-weighting procedure to produce weighted, background-subtracted spectra.

We find that the γ-ray emission consists of two pulses with a total duration of $T_{90} = 0.47 \pm 0.05$ s (15–350 keV; Figure 1), classifying GRB 111117A as a short burst. The spectral time-lag between the 100–350 and 25–50 keV bands is (0.6 ± 2.4) ms, typical of short GRBs (Sakamoto et al. 2011a). The time-averaged spectrum in the 15–150 keV range is best fit by a single power-law model with a hard power-law index, $\Gamma_\gamma = 0.59 \pm 0.14$. The γ-ray fluence derived from this spectrum is $F_\gamma = (1.3 \pm 0.2) \times 10^{-7}$ erg cm^{-2} in the 15–150 keV band, in agreement with the values reported by Sakamoto et al. (2011a) and Mangano et al. (2011b).

The *Fermi*/GBM spectrum in the energy range 10–1000 keV is best fit by a power law with an exponential cutoff, with $\Gamma_\gamma = 0.69 \pm 0.16$ (Foley & Jenke 2011); this is consistent with the BAT spectrum. The peak energy is $E_{\rm pk} \gtrsim 370$ keV, while the observed exponential cutoff indicates that $E_{\rm pk} \lesssim 1$ MeV. The 10–1000 keV band fluence derived from this spectrum is $F_\gamma = (6.7 \pm 0.2) \times 10^{-7}$ erg cm^{-2}. We refer to Sakamoto et al. (2012) for a detailed analysis of the *Fermi*/GBM data.

2.2. X-Ray Observations

We analyzed the data using HEASOFT (v6.11) with standard filtering and screening criteria, and generated the 0.3–10 keV count-rate light curve following the procedures in Margutti et al. (2012). Our rebinning scheme ensures a minimum signal-to-noise ratio (S/N) = 3 for each temporal bin. The low count statistics of the Windowed Timing (WT) observations do not allow us to constrain the spectral parameters during the interval $\delta t \approx 80$–87 s. We model the time-averaged spectrum in the interval 87 s to 40 ks (total exposure of about 9 ks in the Photon Counting mode[6]) with an absorbed power-law model ($tbabs * ztbabs * pow$ within `Xspec`) with a best-fit spectral photon index of $\Gamma_x = 2.0 \pm 0.2$ and an intrinsic neutral hydrogen column density of $N_{\rm H,int} = (6.7 \pm 3.0) \times 10^{21}$ cm^{-2} (C − stat = 98 for 152 dof) in excess to the Galactic column density, $N_{\rm H,MW} = 3.7 \times 10^{20}$ cm^{-2} (Kalberla et al. 2005); we adopt the best-fit photometric redshift of $z = 1.3$ derived in Section 3.1. From the best-fit spectrum we derive an unabsorbed count-to-flux conversion factor of 6.5×10^{-11} erg cm^{-2} counts^{-1} (0.3–10 keV). Uncertainties arising from the flux calibration procedure have been propagated into the individual error bars.

We analyzed the public *Chandra* data (PI: Sakamoto) with the `CIAO` software package (v4.3), using the calibration database CALDB v4.4.2, and applying standard ACIS data filtering. Using `wavdetect` we detect a source at 3.4σ significance at a position consistent with the XRT afterglow, with a net count rate of $(3.3 \pm 1.3) \times 10^{-4}$ counts s^{-1} (0.5–8 keV; total exposure time of 19.8 ks). Assuming the spectral parameters from the XRT analysis, this translates to an unabsorbed flux of $(3.5 \pm 1.4) \times 10^{-15}$ erg s^{-1} cm^{-2} (0.3–10 keV).

The X-ray light curve (Figure 6) exhibits an overall single power-law decay, with an apparent flare at $\delta t \approx 150$ s ($\approx 3\sigma$

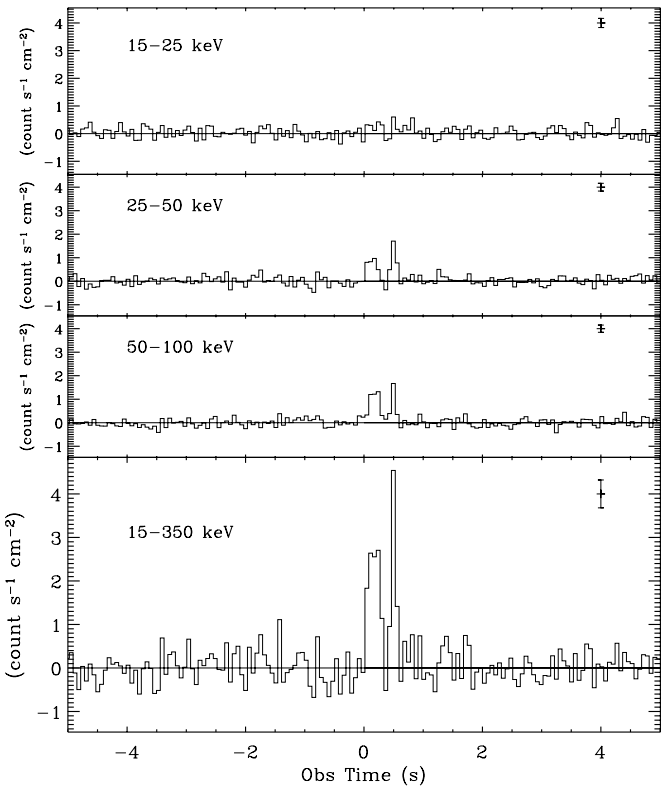

Figure 1. *Swift*/BAT mask-weighted light curve in different energy bands (binning time of 64 ms). The typical 1σ error bar is shown in each panel.

[6] See Hill et al. (2004) for *Swift*/XRT observing modes.

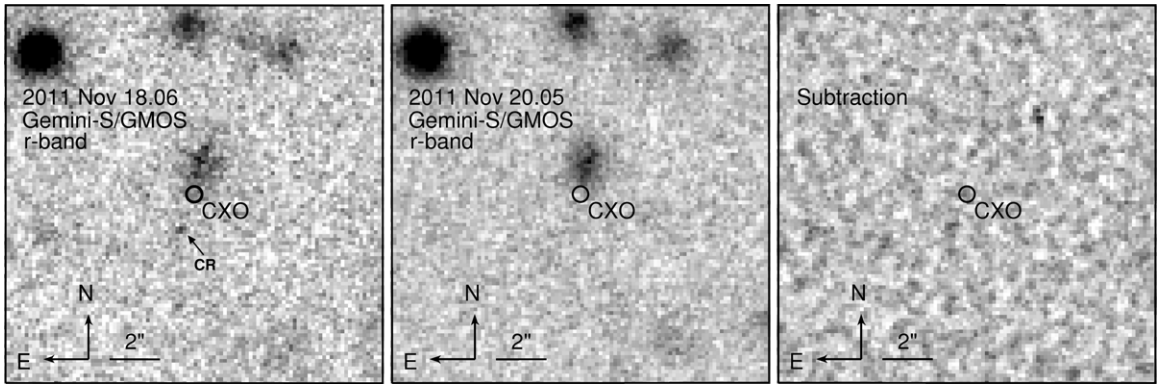

Figure 2. Gemini-South *r*-band observations of GRB 111117A at $\delta t \approx 0.55$ days (left) and ≈2.54 days (middle). Digital image subtraction of the two observations (right) reveals no fading source coincident with the *Chandra* position (circle) or the host galaxy. We note that the apparent emission southeast of the *Chandra* position in the first epoch is a cosmic ray (CR).

confidence level). The best-fit power-law index at $\delta t \gtrsim 300$ s is $\alpha_x = -1.21 \pm 0.05$ ($\chi^2 = 7.6$ for 11 dof).[7]

2.3. Optical Afterglow Limits

We obtained deep *r*-band observations with the Gemini Multi-Object Spectrograph (GMOS; Hook et al. 2004) mounted on the Gemini-South 8 m telescope on 2011 November 18.06 and 20.05 UT, with total exposure times of 1800 s and 2880 s, respectively. We processed the data using the `gemini` package in IRAF,[8] and calibrated the photometry with several nearby point sources from the Sloan Digital Sky Survey (SDSS; Abazajian et al. 2009). We further performed digital image subtraction of the two epochs using the High Order Transformation and Point Spread Function and Template Subtraction (HOTPANTS[9]), but no fading source is detected within the XRT error circle, or in coincidence with the putative host galaxy to $r \gtrsim 25.5$ mag (3σ) at $\delta t \approx 0.55$ days (Figure 2). We note that this is the deepest limit to date on the early optical emission from a short GRB (Berger 2010; Fong et al. 2011a), with the exception of GRB 080503 which was eventually detected at $\delta t \gtrsim 1$ day (Perley et al. 2009). Indeed, the median optical afterglow brightness for detected short GRBs on a similar timescale is $r \approx 23.5$ mag, a factor of at least six times brighter (Berger 2010; Fong et al. 2011a).

2.4. X-Ray/Optical Differential Astrometry

In the absence of an optical afterglow, we use the *Chandra* observation to refine the *Swift*/XRT position to subarcsecond accuracy. We perform differential astrometry between the *Chandra* data and a Gemini-North *i*-band observation (Section 2.5) to determine the relative positions of the afterglow and host galaxy, as well as to refine the native *Chandra* astrometry. We use `SExtractor`[10] to determine the positions and centroid uncertainties of sources in the GMOS image. Performing an absolute astrometric tie to the SDSS catalog using

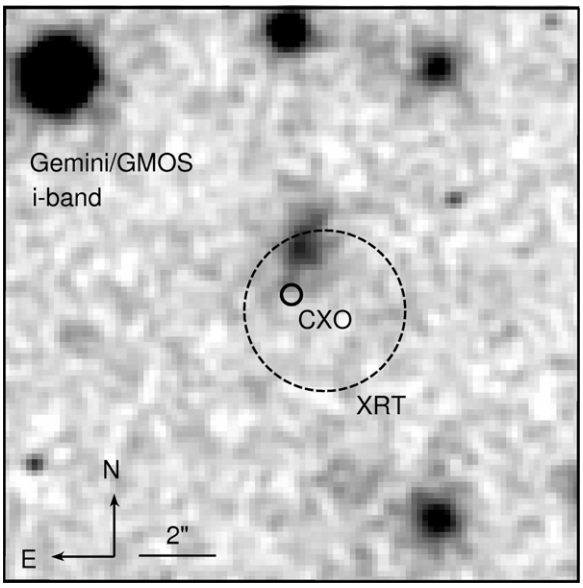

Figure 3. Gemini/GMOS *i*-band image of a $15'' \times 15''$ field centered on the *Chandra* position of the X-ray afterglow of GRB 111117A (solid circle; 90% confidence region). Also shown is the *Swift*/XRT position (dashed circle; 90% confidence region). The host galaxy is clearly detected with an offset of about $1''.25$ from the *Chandra* position.

71 common point sources, we find a resulting rms value of $\sigma_{\rm GMOS\text{-}SDSS} = 0''.13$ ($0''.09$ in each coordinate).

To refine the native *Chandra* astrometry and to determine the location of the X-ray afterglow relative to the GMOS image, we perform differential astrometry. We use the `CIAO` routine `wavdetect` to obtain positions and 1σ centroid uncertainties of X-ray sources in the field, including the afterglow of GRB 111117A, with a resulting $\sigma_{\rm X,ag} = 0''.13$. We calculate an astrometric tie based on two X-ray and optically bright common sources and find weighted mean offsets of δR.A. $= -0''.18 \pm 0''.03$ and δdecl. $= -0''.02 \pm 0''.11$ giving a tie uncertainty[11] of $\sigma_{\rm Chandra-GMOS} = 0''.12$. Applying the astrometric solution, we obtain a *Chandra* afterglow position of R.A. $= 00^{\rm h}50^{\rm m}46^{\rm s}.283$ and decl. $= +23^\circ00'39''.64$; see Figure 3. The total 1σ uncertainty in the absolute position is $0''.22$, accounting for the SDSS–GMOS astrometric tie, GMOS–*Chandra* tie,

[7] The power-law index is obtained by minimizing the integral of the model over the effective duration of each temporal bin of the light curve. This procedure is of primary importance in the case of bins with long duration and produces more accurate results than the standard χ^2 procedure, which compares the model and the data at the nominal bin time, but does not consider the finite bin duration and the evolution of the model during the time interval.

[8] IRAF is distributed by the National Optical Astronomy Observatory, which is operated by the Association for Research in Astronomy, Inc., under cooperative agreement with the National Science Foundation.

[9] http://www.astro.washington.edu/users/becker/hotpants.html.

[10] http://sextractor.sourceforge.net/

[11] There are two additional fainter common sources, which lead to increased scatter in the astrometric tie without changing the absolute value, and we therefore use only the two bright sources.

Table 1
GRB 111117A Host Galaxy Optical and NIR Photometry

Date (UT)	Δt (days)	Telescope	Instrument	Filter	Exposures (s)	$\theta_{\rm FWHM}$ (arcsec)	Host[a] (AB mag)	A_λ (AB mag)
2011 Nov 18.08	0.57	Magellan/Baade	IMACS	r	4×300	1.06	23.72 ± 0.11	0.069
2011 Nov 28.13	10.62	MPG/ESO	GROND	g	8×375	1.07	24.14 ± 0.18	0.120
2011 Nov 28.25	10.74	Gemini-North	GMOS	i	10×180	0.75	23.66 ± 0.08	0.051
2011 Nov 28.27	10.76	Gemini-North	GMOS	z	10×180	0.83	23.04 ± 0.18	0.038
2011 Dec 7.07	19.56	Magellan/Baade	FourStar	J	15×60	0.78	22.55 ± 0.30	0.027
2011 Dec 7.05	19.54	Magellan/Baade	FourStar	K_s	10×90	0.68	$\gtrsim 22.10$	0.011

Note. [a] These values have been corrected for Galactic extinction, A_λ (Schlafly & Finkbeiner 2011).

and the X-ray afterglow positional uncertainty. The *Chandra* position is consistent with the XRT position, but refines its uncertainty by about a factor of 6. We note that the *relative* position of the X-ray afterglow in the GMOS astrometric frame is 0.″18 (GMOS–*Chandra* tie and afterglow positional uncertainty only).

2.5. Host Galaxy Optical/Near-IR Observations

We obtained optical observations in the $griz$ bands, and near-IR observations in JK_s bands to determine the properties of the host galaxy. The details of the observations are summarized in Table 1. The g-band observation was performed with GROND (Greiner et al. 2008) mounted at the 2.2 m MPG/ESO telescope at La Silla Observatory (Chile). The r-band observation was obtained with the Inamori-Magellan Areal Camera and Spectrograph (IMACS) on the Magellan/Baade 6.5 m telescope, while the iz band observations were performed with GMOS mounted on the Gemini-North 8 m telescope. Finally, the JK_s-band observations were obtained with the FourStar wide-field near-IR camera on the Magellan/Baade telescope. The GMOS data were reduced using the `gemini` package in IRAF, the IMACS and GROND data were reduced using standard packages in IRAF, and the FourStar data were reduced using a custom pipeline in python.

We identify a galaxy near the *Chandra* position, at R.A. = $00^{\rm h}50^{\rm m}46\overset{\rm s}{.}267$ and decl. = $+23^\circ00'40\overset{''}{.}87$ (astrometry relative to SDSS; Section 2.4), with a centroid uncertainty of 0.″08. The offset between the galaxy centroid and the *Chandra* afterglow position is $1\overset{''}{.}25 \pm 0\overset{''}{.}20$. Photometry of the galaxy is performed in a 2″ radius aperture, with the zero-point determined by common sources with SDSS ($griz$) and Two Micron All Sky Survey (JK_s). The resulting magnitudes are listed in Table 1.

To determine the probability of chance coincidence for this galaxy relative to the afterglow position, we adopt the methodology of Bloom et al. (2002) and Berger (2010). The expected number density of galaxies brighter than the apparent magnitude of the galaxy, $m_r = 23.6$ mag, is (Hogg et al. 1997; Beckwith et al. 2006):

$$\sigma(\leqslant m) = \frac{1}{0.33 \times \ln(10)} \times 10^{0.33(m_r - 24) - 2.44} \approx 0.004\,{\rm arcsec}^{-2}, \quad (1)$$

and the probability of chance coincidence is therefore:

$$P(<\delta R) = 1 - {\rm e}^{-\pi(\delta R)^2 \sigma(\leqslant m_r)} \approx 0.02. \quad (2)$$

Given the low value of $P(<\delta R)$ and the absence of other candidate hosts in the vicinity of the afterglow position, we consider this galaxy to be the host of GRB 111117A. We note that with the XRT position alone the probability of chance coincidence for this galaxy is much larger, $P(<\delta R) \approx 0.17$ (using $\delta R \approx 3\sigma_{\rm X,XRT}$; see Bloom et al. 2002).

2.6. Radio Observations

We observed the location of GRB 111117A with the Karl G. Jansky Very Large Array (Perley et al. 2011) on 2011 November 18.00 UT ($\delta t \approx 0.5$ days) at a mean frequency of 5.8 GHz with a total on-source integration time of 75 minutes. We used 3C48 and J0042+2320 for bandpass/flux and gain calibration, respectively, and followed standard procedures in the Astronomical Image Processing System (AIPS; Greisen 2003) for data calibration and analysis. The effective bandwidth is about 1.5 GHz after excising edge channels and data affected by radio frequency interference. We reflagged and calibrated our data after the initial quick reduction (Fong et al. 2011c) and do not detect any significant emission in coincidence with the *Chandra* position to a 3σ limit of 18 μJy.

3. RESULTS AND DISCUSSION

3.1. Host Galaxy Properties

To determine the photometric redshift and properties of the host galaxy, we use our $grizJK_s$ band photometry. We model the host spectral energy distribution (SED) with the Maraston (2005) evolutionary stellar population synthesis models, using a Salpeter initial mass function, solar metallicity, and a red horizontal branch morphology, with the redshift (z) and stellar population age (τ) as free parameters. The resulting best-fit model is shown in Figure 4, along with the confidence regions for the redshift and age. We find that $z = 1.3^{+0.3}_{-0.2}$ and $\tau = 70^{+65}_{-40}$ Myr ($\chi^2 = 1.2$ for 3 dof); the results remain unchanged if we use a model with a metallicity of 0.5 $Z_\odot$. The inferred redshift is consistent with the independent estimate by Sakamoto et al. (2012) and is one of the highest for any short GRB to date, either from spectroscopic or photometric measurements (Levan et al. 2006a; de Ugarte Postigo et al. 2006; Berger et al. 2007; Graham et al. 2009; Leibler & Berger 2010), but is in the range of expected redshifts for short GRBs with faint hosts (Berger et al. 2007).

The inferred stellar population age is at the low end of the distribution for short GRB hosts, for which $\langle\tau\rangle \approx 0.3$ Gyr (Leibler & Berger 2010). The inferred host galaxy stellar mass is $M_* \approx 4 \times 10^9\,M_\odot$, about a factor of three times lower than the median for short GRB hosts, but this assumes a single stellar population. Contribution from an older stellar population could increase the total mass up to a maximal value of $\approx 7 \times 10^{10}\,M_\odot$ if we assume the presence of a stellar population with the age of the universe at $z = 1.3$ (c.f., Leibler & Berger 2010). We note that the stellar population age and specific star formation

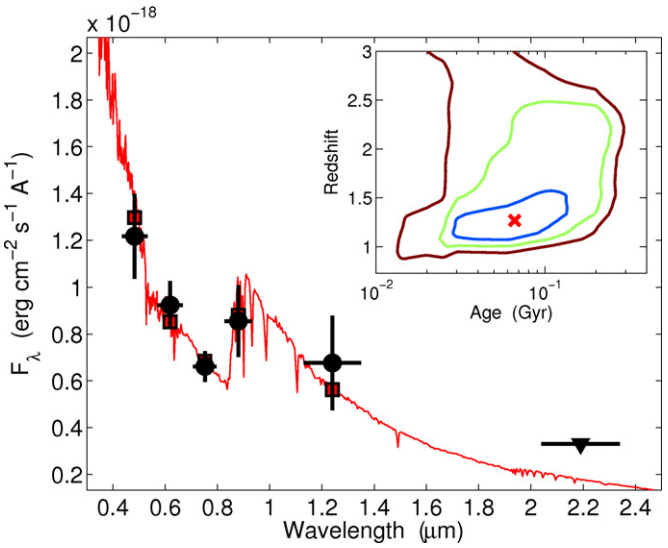

Figure 4. Optical and near-IR spectral energy distribution of the host galaxy of GRB 111117A (black), along with the Maraston (2005) evolutionary stellar population synthesis models. The best-fit model (red squares and line) has a photometric redshift of $z \approx 1.3$ and a stellar population age of $\tau \approx 70$ Myr (the inset).

(A color version of this figure is available in the online journal.)

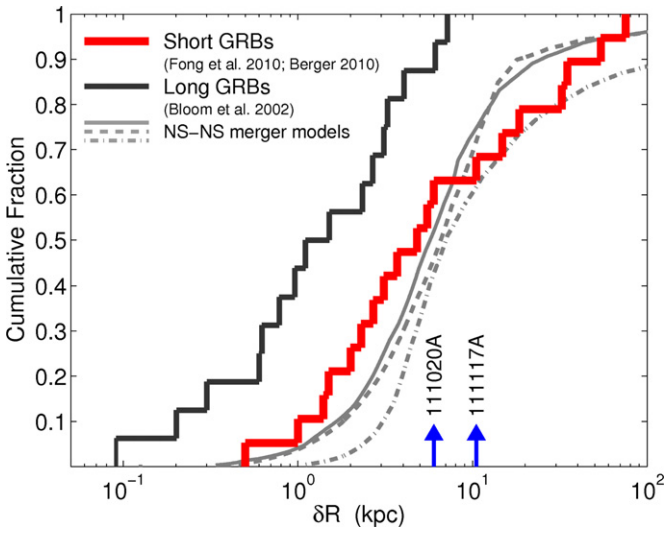

Figure 5. Cumulative distribution of projected physical offsets for short GRBs with subarcsecond positions (red; Fong et al. 2010; Berger 2010; Fong et al. 2012), including GRB 111117A, and for long GRBs (black; Bloom et al. 2002). Also shown are population synthesis model predictions for NS–NS binaries (Bloom et al. 1999; Fryer et al. 1999; Belczynski et al. 2006). Arrows mark the offsets of the two short GRBs localized by *Chandra* alone, GRB 111117A from this work and GRB 111020A from Fong et al. (2012). These offsets are somewhat larger than the median short GRB offset of about 5 kpc.

(A color version of this figure is available in the online journal.)

rate are similar to those of long GRB host galaxies, for which $\langle\tau\rangle \approx 60$ Myr and $\langle \mathrm{SFR}/L_B\rangle \approx 10\,M_\odot\ \mathrm{yr}^{-1} L_B^{*-1}$ (Berger 2009; Leibler & Berger 2010).

From the observed g-band flux density, which samples the rest-frame UV luminosity, we infer a star formation rate of $\mathrm{SFR} \approx 6\,M_\odot\ \mathrm{yr}^{-1}$ (Kennicutt 1998). This is higher than for most previous short GRB host galaxies (Berger 2009). The absolute B-band magnitude is $M_B \approx -21.0$ mag, corresponding to $L_B \approx 0.6\,\mathrm{L}^*$ in comparison to the DEEP2 luminosity function at $z \approx 1.1$ (Willmer et al. 2006); this value is typical for short GRB hosts (Berger 2009). Combining the star formation rate and B-band luminosity, we infer a specific star formation rate of $\mathrm{SFR}/L_B \approx 10\,M_\odot\ \mathrm{yr}^{-1}\ L_B^{*-1}$. This is again at the upper end of the distribution for short GRB host galaxies (Berger 2009).

The host galaxy of GRB 111117A is overall similar to the host of short GRB 060801 ($z = 1.130$) in terms of its star formation rate and stellar mass (Berger 2009). It provides additional support to the conclusion that short GRB progenitors originate from diverse stellar populations. Under the assumption that the stellar population ages can be used as a proxy for the progenitor delay time distribution (Leibler & Berger 2010), events like GRB 111117A point to delay times as short as a few tens of Myr. In the context of neutron star (NS)–NS/NS–black hole (BH) mergers, this is suggestive of a subset of short-lived compact object binaries (e.g., Belczynski & Kalogera 2001; Belczynski et al. 2002).

3.2. Offset

The *Chandra*-derived projected angular offset of $1\farcs25 \pm 0\farcs20$ corresponds to a projected physical offset of $\delta R = 10.5 \pm 1.7$ kpc at $z = 1.3$. This is comparable to the median offset of about 5 kpc for the sample of short GRBs studied by Fong et al. (2010) and Berger (2010; see Figure 5). Indeed, as a subset, the two short bursts with precise localizations from *Chandra* alone (GRB 111020A from Fong et al. 2012 and GRB 111117A presented here) have similar offsets to those inferred from optical afterglows. This suggests that optical afterglows do not produce an obvious bias against large offsets, as already demonstrated for the subset of short GRBs that lack coincident host galaxies (Berger 2010).

Different short GRB progenitor models predict distinct offset distributions. NS–NS/NS–BH merger models predict a median offset of about 5–10 kpc (Bloom et al. 1999; Fryer et al. 1999; Belczynski et al. 2006) for host galaxies with a mass comparable to the Milky Way as found for short GRBs (Berger 2009). On the other hand, magnetar models are not expected to produce a substantial fraction of short GRBs at offsets of $\gtrsim$10 kpc (Levan et al. 2006b; Metzger et al. 2008). Figure 5 shows that NS–NS binary models are in reasonable agreement with the observed distribution of physical offsets, from both optical and *Chandra* positions.

3.3. X-Ray Afterglow Properties

At $z = 1.3$ the X-ray afterglow of GRB 111117A lies at the upper end of the short GRB luminosity distribution, with a typical power-law decay (Figure 6). The total energy released in the 0.3–10 keV energy band during the X-ray afterglow (80 s to 3 days) is $E_{\mathrm{x,iso}} = (1.1 \pm 0.1) \times 10^{50}$ erg, typical for short GRBs (the Figure 6 inset). This confirms previous findings that the X-ray afterglows of short GRBs are on average $\sim$100 times less energetic than those of long GRBs (Margutti et al. 2012). The corresponding energy radiated in the 0.3–30 keV rest-frame band[12] is $E_{\mathrm{x,iso}} \approx 1.5 \times 10^{50}$ erg. In comparison to the isotropic γ-ray energy this indicates $E_{\mathrm{x,iso}} \approx 0.03 E_{\gamma,\mathrm{iso}}$, which is typical of short GRBs.[13]

We combine this result with the inferred rest-frame value of $E_{\mathrm{pk}} \sim$ 850–2300 keV to show that GRB 111117A is consistent

[12] This value is obtained by extrapolating the spectral behavior in the 0.3–10 keV observer frame range (0.7–23 keV rest frame) to the 0.3–30 keV rest-frame range.

[13] We assumed a high energy photon index $\beta = -2.4$ (see e.g., Kaneko et al. 2006) to extrapolate the 23–2300 keV (rest-frame) spectrum to the 1–10^4 keV rest-frame range.

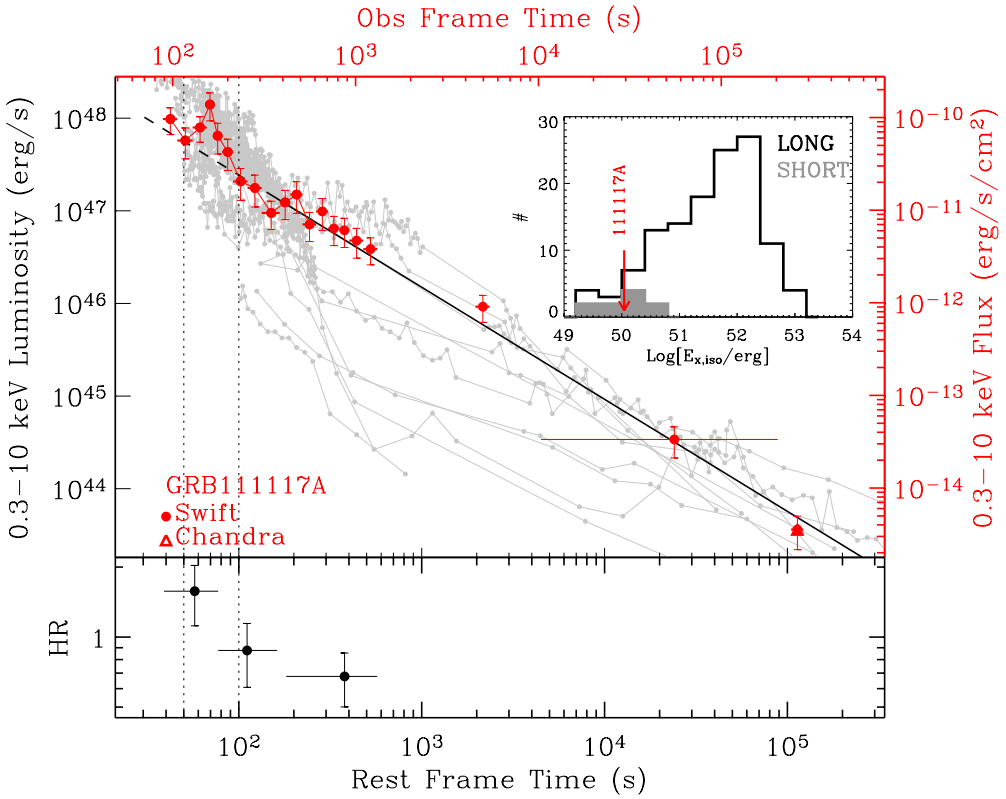

Figure 6. Upper panel: unabsorbed 0.3–10 keV flux and luminosity light curve of GRB 111117A (red dots: *Swift*/XRT; red triangle: *Chandra*) compared to 11 short GRBs detected by *Swift* for which a redshift measurement is available (gray lines). The best-fit power-law model has $\alpha_x = -1.21 \pm 0.05$ (solid black line). An apparent flare is detected at ≈80–200 s (black dotted lines). The inset shows the distribution of the isotropic energy emitted during the X-ray afterglow for long GRBs (black line) and short GRBs (gray filled histogram) as computed by Margutti et al. (2012). For GRB 111117A we measure $E_{\rm x,iso} \approx 1.1 \times 10^{50}$ erg s^{-1}. Lower panel: time evolution of the hardness ratio measured between the 1.5–10 keV and the 0.3–1.5 keV energy bands.

(A color version of this figure is available in the online journal.)

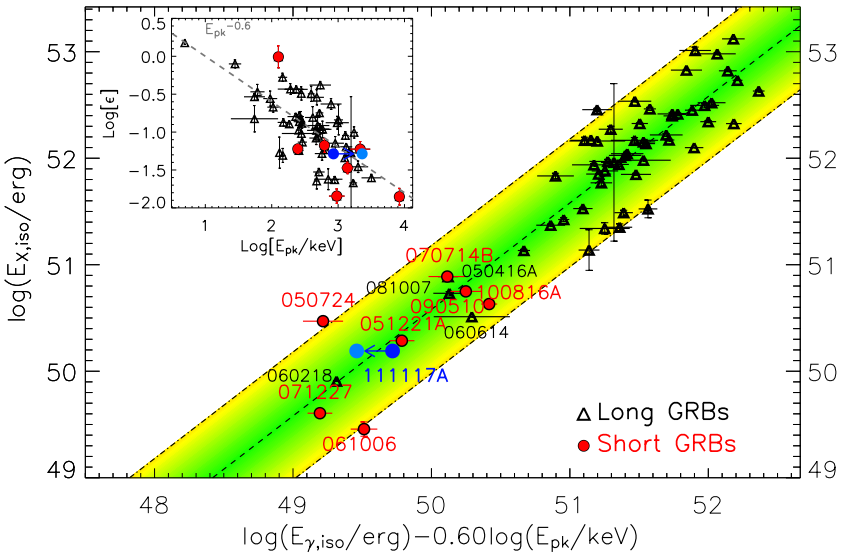

Figure 7. Three-parameter correlation involving the isotropic energy emitted in the X-ray afterglow ($E_{\rm x,iso}$; rest-frame 0.3–30 keV), the isotropic γ-ray energy ($E_{\gamma,\rm iso}$; rest-frame 1–10^4 keV), and the rest-frame spectral peak energy during the prompt phase ($E_{\rm pk}$). The blue circles mark GRB 111117A using the range of $E_{\rm pk} \sim 850$–2300 keV (Section 2.1). The dot-dashed lines mark the 90% confidence area around the best-fit relation: $E_{\rm x,iso} \propto E_{\gamma,\rm iso}^{1.00\pm0.06}\, E_{\rm pk}^{-0.60\pm0.10}$. The inset shows the evolution of $\epsilon \equiv E_{\rm x,iso}/E_{\gamma,\rm iso}$ as a function of $E_{\rm pk}$. Adapted from Margutti et al. (2012).

(A color version of this figure is available in the online journal.)

with the recently reported $E_{\rm x,iso}$–$E_{\gamma,\rm iso}$–$E_{\rm pk}$ correlation for long and short GRBs, and resides in the region populated by short GRBs and X-ray flashes (Figure 7; Margutti et al. 2012). This provides additional support to the conclusions that (1) this correlation can be used to divide "standard" long GRBs from short GRBs, peculiar GRBs, and X-ray flashes; and (2) the physical origin of the correlation is related to a common feature of the different classes, possibly the properties of the relativistic

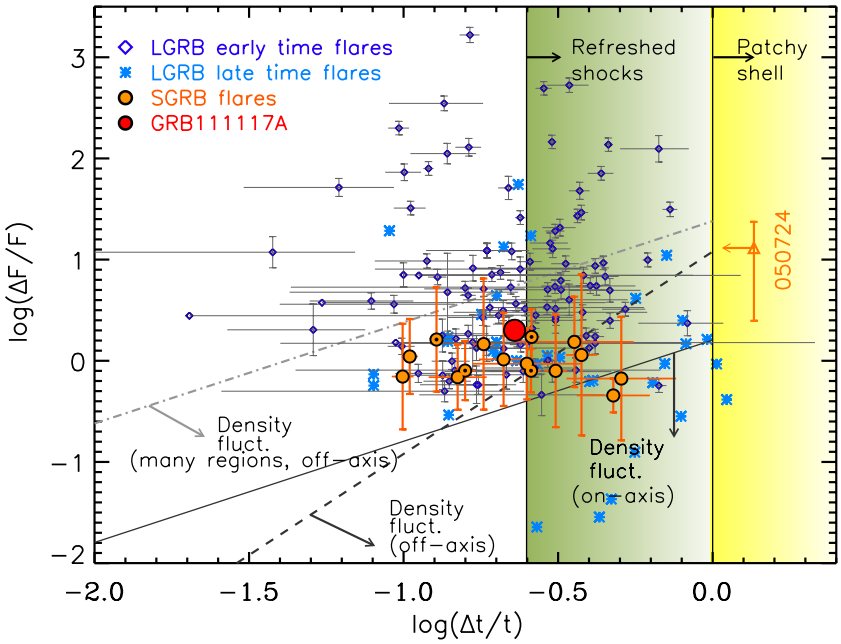

Figure 8. Relative variability flux ($\Delta F/F$) vs. relative variability timescale ($\Delta t/t$) for a sample of short GRB X-ray flare candidates (orange filled circles; Margutti et al. 2011), as well as early- (blue open diamonds; Chincarini et al. 2010) and late-time (light-blue stars; Bernardini et al. 2011) flares in long GRBs. A small black dot marks short GRBs with extended emission. The apparent flare detected in GRB 111117A is marked with a red filled circle. The late-time rebrightening detected in GRB 050724 is also shown for completeness with an orange open triangle. Solid, dashed, and dot-dashed lines mark the kinematically allowed regions according to Ioka et al. (2005, their Equations (7) and (A2)).

(A color version of this figure is available in the online journal.)

outflow (in particular the bulk Lorentz factor; see Bernardini et al. 2012 for details; see Fan et al. 2012 and Dado & Dar 2012 for alternative explanations).

At $\delta t \approx 80$–250 s we find evidence for an apparent flare superimposed on the smooth X-ray afterglow decay, with a significance of $\approx 3\sigma$ (Figure 6). With a rest-frame duration of $\Delta t \approx 16$ s and peak time of $t_{\rm pk} \approx 70$ s, the flare is consistent with the Δt versus $t_{\rm pk}$ correlation established by long GRB flares (Chincarini et al. 2010) and shared by short GRBs flares (Margutti et al. 2011). The flux contrast of the flare, $\Delta F/F \approx 2$, is also typical of flares in short GRBs (Figure 8). Finally, the flare peak luminosity and integrated energy are $L_{\rm pk}^{\rm flare} \approx 10^{48}$ erg s^{-1} and $E_{\rm X}^{\rm flare} \approx 1.6 \times 10^{49}$ erg, again typical of short GRB flares (Margutti et al. 2011). We note that the value of $\Delta t/t_{\rm pk} \approx 0.2$ does not support an external shock origin, for which we expect $\Delta t/t_{\rm pk} \gtrsim 1$ (e.g., Zhang et al. 2006; but see Dermer 2008). However, the flux contrast of $\Delta F/F \approx 2$ is also at odds with the expectation for central engine variability, with $\Delta F/F \approx 100$ (Lazzati et al. 2011).

3.4. Multi-wavelength Afterglow Modeling

The detected X-ray afterglow, along with the upper limits in the optical and radio allow us to extract some of the basic properties of GRB 111117A. We adopt the afterglow synchrotron model formulation of Granot & Sari (2002), which provides a mapping from the observed fluxes and break frequencies to the isotropic-equivalent kinetic energy ($E_{\rm K,iso}$), circumburst density (n_0), the fractions of post-shock energy in radiating electrons (ϵ_e) and magnetic fields (ϵ_B), and the electron power-law distribution index (p, with $N(\gamma) \propto \gamma^{-p}$). We consider the case of a constant density medium relevant for short GRBs. In the analysis below we adopt the best-fit redshift of $z = 1.3$.

The X-ray temporal and spectral indices are $\alpha_X = -1.21 \pm 0.05$ and $\beta_X = -1.0 \pm 0.2$ (Section 2.2). For the case of the synchrotron cooling break located redward of the X-ray band ($\nu_c < \nu_X$), the resulting values of p are 2.28 ± 0.07 and 2.0 ± 0.4 from α_X and β_X, respectively; for the opposite scenario ($\nu_c > \nu_X$) the resulting values of p are 2.61 ± 0.07 and 3.0 ± 0.4. In both cases the values of p inferred from α_X and β_X are consistent, indicating that the X-ray data alone cannot distinguish the location of ν_c.

The unabsorbed X-ray flux density at the time of the optical non-detection ($\delta t \approx 0.55$ days) is $F_{\nu,\rm X} \approx 4.4$ nJy, compared with $F_{\nu,\rm opt} \lesssim 0.23$ μJy. This leads to an observed spectral index of $\beta_{\rm OX} \gtrsim -0.63$, consistent with the value of $p \approx 2.28$ for the case of $\nu_c < \nu_X$, if $\nu_c \approx \nu_X$ (i.e., if the relevant spectral slope between the X-ray and optical bands is $\beta_{\rm OX} = -(p-1)/2$). On the other hand, if $\nu_c > \nu_X$ we expect a spectral index of $\beta_{\rm OX} = -(p-1)/2 \approx -0.80$, which is much steeper than the observed value. With this spectral index we would expect the optical flux to be ≈ 0.65 μJy, or about 1.1 mag brighter than the observed limit. Thus, the X-ray/optical comparison either requires rest-frame extinction of $A_V^{\rm host} \gtrsim 0.5$ mag or $\nu_c \approx \nu_X$. We note that for the Galactic relations between N_H and A_V (Predehl & Schmitt 1995) the optical extinction would imply $N_H^{\rm host} \gtrsim 10^{21}$ cm^{-2}, consistent with the marginal detection in the XRT spectrum of $(6.7 \pm 3.0) \times 10^{21}$ cm^{-2}.

Under the assumption that $\nu_c < \nu_X$ we can use the *Chandra* X-ray flux density, $F_{\nu,\rm X} \approx 0.42$ nJy, to infer the value of the isotropic-equivalent kinetic energy:

$$E_{\rm K,iso} \approx 7.5 \times 10^{50}\,{\rm erg}, \quad (3)$$

where we have assumed $\epsilon_e = \epsilon_B = 0.1$; we note that the dependence on ϵ_B is weak, $E_{\rm K,iso} \propto \epsilon_B^{-0.07}$, while $E_{\rm K,iso}$ is inversely proportional to ϵ_e. The fiducial value of $E_{\rm K,iso}$ is lower than the isotropic-equivalent γ-ray energy, $E_{\gamma,\rm iso} \approx 3.0 \times 10^{51}$ erg.

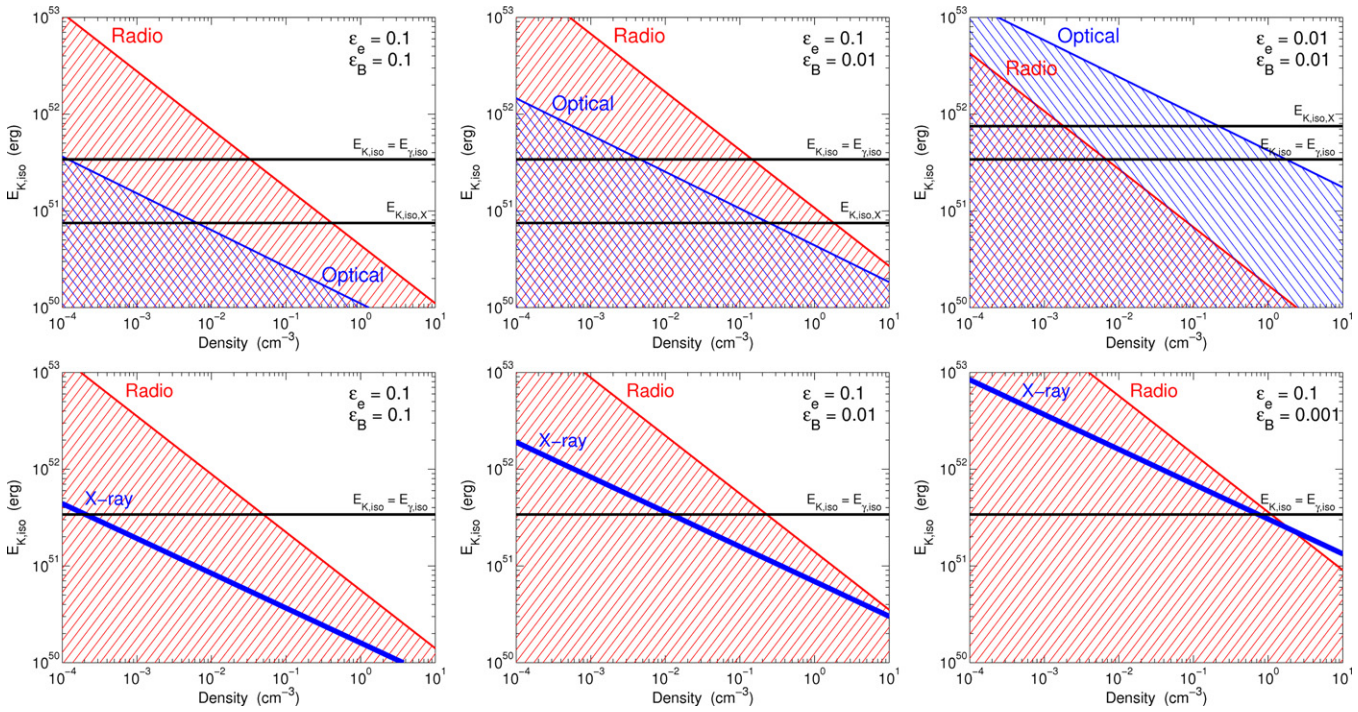

Figure 9. Phase-space of isotropic-equivalent blastwave kinetic energy and circumburst density delineated by the X-ray detection (thick line) and the optical and/or radio upper limits (hatched regions). The top row is for the case $\nu_c < \nu_X$, with the X-ray detection providing a measure of the $E_{\rm K,iso}$ (horizontal line). The bottom row is for the case $\nu_c > \nu_X$ for which the optical limit is redundant with respect to the X-ray detection. Here the case of $E_{\rm K,iso} = E_{\gamma,\rm iso}$ is marked by the horizontal black line. The panels are for different combinations of ϵ_e and ϵ_B.

(A color version of this figure is available in the online journal.)

We next use the upper bounds on the radio and optical flux densities to place constraints on the circumburst density and energy. For the radio upper limit we use the synchrotron flux density relevant for $\nu_a < \nu_{\rm rad} < \nu_m$:

$$F_{\nu,\rm rad} \approx 36\,\mu{\rm Jy}\,n_0^{1/2}\,E_{\rm K,iso,51}^{5/6} \lesssim 18\,\mu{\rm Jy}, \quad (4)$$

while for the optical upper limit we use the synchrotron flux density relevant for $\nu_m < \nu_{\rm opt} < \nu_c$:

$$F_{\nu,\rm opt} \approx 4.4\,\mu{\rm Jy}\,n_0^{1/2}\,E_{\rm K,iso,51}^{1.32} \lesssim 0.23\,\mu{\rm Jy}. \quad (5)$$

The resulting allowed phase-space of $E_{\rm K,iso}$ and n_0 is shown in Figure 9. Using the value of $E_{\rm K,iso}$ inferred from the X-ray data (Equation (3)), and the corresponding limits on n_0 from the optical data ($n_0 \lesssim 0.006$ cm^{-3}) and radio data ($n_0 \lesssim 0.4$ cm^{-3}), we find that the cooling frequency is located at $\nu_c \gtrsim (0.15\text{–}8) \times 10^{17}$ Hz (i.e., $\gtrsim$0.06–3 keV) at $\delta t = 1000$ s. Using instead a value of $\epsilon_B = 0.01$ the limits on the density are $\lesssim$0.25 cm^{-3} (optical) and $\lesssim$2 cm^{-3} (radio), and the cooling frequency is therefore $\nu_c \gtrsim (0.9\text{–}7) \times 10^{17}$ Hz (i.e., $\gtrsim$0.4–3 keV). Thus, the inferred location of ν_c is in the X-ray band, in agreement with our conclusion from the comparison of X-ray and optical flux densities.

In the alternative scenario of $\nu_c > \nu_X$ both the optical and X-ray bands probe the same portion of the synchrotron spectrum, $\nu_m < \nu_{\rm opt,X} < \nu_c$, but this time with a value of $p = 2.61$. For the X-ray band, this gives the relation (for $\epsilon_e = \epsilon_B = 0.1$):

$$F_{\nu,\rm X} \approx 4.4\,{\rm nJy}\,n_0^{1/2}\,E_{\rm K,iso,51}^{1.4} \approx 0.42\,{\rm nJy}, \quad (6)$$

while for the radio band ($\nu_a < \nu_{\rm rad} < \nu_m$) we find

$$F_{\nu,\rm rad} \approx 12\,\mu{\rm Jy}\,n_0^{1/2}\,E_{\rm K,iso,51}^{5/6} \lesssim 18\,\mu{\rm Jy}. \quad (7)$$

The resulting allowed regions of $E_{\rm K,iso} - n_0$ phase-space are shown in Figure 9. Assuming that $E_{\rm K,iso} = E_{\gamma,\rm iso} = 3.0 \times 10^{51}$ erg, the X-ray flux density corresponds to $n_0 \approx 3 \times 10^{-4}$ cm^{-3}; for $\epsilon_B = 0.01$ the density is instead[14] $\approx$0.02 cm^{-3}, while for $\epsilon_B = 0.001$ the density is $\approx$1.2 cm^{-3}. With these values we indeed find that $\nu_c \gtrsim 4 \times 10^{18}$ Hz ($\gtrsim$16 keV) at $\delta t = 1000$ s, consistent with the assumption that $\nu_c > \nu_X$.

To conclude, with the assumption that $\nu_c < \nu_X$ we find that $E_{\rm K,iso} \approx 7.5 \times 10^{50}$ erg, and $n_0 \lesssim 0.01$ cm^{-3} ($\epsilon_B = 0.1$) or $\lesssim$0.2 cm^{-3} ($\epsilon_B = 0.01$). The resulting location of the cooling break indicates that $\nu_c \sim \nu_X$, marginally consistent with the inherent assumption. On the other hand, if $\nu_c > \nu_X$, then the assumption of $E_{\rm K,iso} \approx E_{\gamma,\rm iso}$ indicates that $n_0 \approx 3 \times 10^{-4} - 1$ cm^{-3} (for $\epsilon_B = 0.001$–0.1). However, this also requires host galaxy extinction with $A_V^{\rm host} \gtrsim 0.5$ mag. In both cases the inferred density is consistent with the NS–NS/NS–BH merger scenario, for which the expected densities are $n_0 \sim 10^{-6} - 1$ cm^{-3} (Perna & Belczynski 2002; Belczynski et al. 2006).

Finally, the non-detection of a break in the X-ray light curve to $\delta t \approx 3$ days allows us to place a lower limit on the opening angle of the outflow from GRB 111117A. Using the formulation of (Frail et al. 2001)[15] we find that for $E_{\rm K,iso} = E_{\gamma,\rm iso}$ and $n_0 \approx 3 \times 10^{-4} - 1$ cm^{-3}, the resulting lower limit is $\theta_j \gtrsim$ 3–10°. This range indicates a beaming correction as low as $\approx$70 and as high as about 600.

[14] We can rule out $\epsilon_e = \epsilon_B = 0.01$ or $\epsilon_e = 0.1$ and $\epsilon_B \lesssim 0.001$ since in these cases the upper limit on the density from the radio data is lower than the density inferred from the X-ray detections.

[15] In this calculation the observer is assumed to be on-axis.

4. SUMMARY AND CONCLUSIONS

We presented multi-wavelength observations of the afterglow of short GRB 111117A, along with optical and near-IR follow-up observations of its host galaxy. These observations provide critical insight into the nature of GRB 111117A:

1. Using a *Chandra* observation we accurately pinpoint the location of the afterglow to the outskirts of a galaxy at a photometric redshift of $z \approx 1.3$, one of the highest for any short GRB to date. The projected physical offset is about 10.5 kpc, reminiscent of previous short GRBs (Fong et al. 2010; Berger 2010). Along with the previous burst detected by *Chandra* alone (GRB 111020A; Fong et al. 2012), we find that short GRBs localized by optical and X-ray afterglows appear to have similar offsets.
2. The host galaxy of GRB 111117A exhibits vigorous star formation activity and a young stellar population age that are at the upper bound of the distribution for short GRB hosts (Berger 2009; Leibler & Berger 2010).
3. The X-ray afterglow properties are typical of short GRBs with long-lasting X-ray emission. In particular, with $E_{\rm x,iso} \approx 1.5 \times 10^{50}$ erg, $E_{\gamma,\rm iso} \approx 3 \times 10^{51}$ erg, and $E_{\rm pk} \approx 850$–2300 keV, GRB 111117A is consistent with the three-parameter universal GRB scaling recently reported by Margutti et al. (2012). The X-ray to γ-ray energy ratio for GRB 111117A is $\epsilon \approx 0.03$, as typically found for short GRBs.
4. We find evidence (statistical significance of $\sim 3\sigma$) for an early flare superimposed on the X-ray afterglow decay with properties that are reminiscent of X-ray flare candidates detected in other short GRBs (Margutti et al. 2011). The origin of X-ray flares appears to be independent of the large scale environment since they are detected from short GRBs in both early- and late-type galaxies.
5. Using the X-ray light curve, and deep upper limits in the optical and radio bands we find that if $\nu_c > \nu_X$ then $n_0^{1/2} E_{\rm K,iso,51}^{1.4} \approx 0.1$–$6$ (for $\epsilon_e = 0.1$ and $\epsilon_B = 0.001$–0.1). For the specific case of $E_{\rm K,iso} = E_{\gamma,\rm iso} \approx 3.0 \times 10^{51}$ erg, this leads to a density of $n_0 \approx 3 \times 10^{-4} - 1$ cm^{-3}; larger densities are ruled out independently by the radio limit, which leads to $n_0^{1/2} E_{\rm K,iso,51}^{5/6} \lesssim 0.7$–$3$ (for $\epsilon_e = 0.1$ and $\epsilon_B = 0.001$–0.1). However, this scenario requires substantial rest-frame extinction of $A_V^{\rm host} \gtrsim 0.5$ mag to explain the optical non-detection. In the alternative scenario of $\nu_c < \nu_X$ we find that $E_{\rm K,iso} \approx 7.5 \times 10^{50} (\epsilon_e/0.1)^{-1}$ erg and $n_0 \lesssim 0.1$ cm^{-3}.
6. The lack of a clear break in the X-ray light curve at $\lesssim 3$ days, points to an opening angle of $\theta_j \gtrsim 3$–10°, with the exact lower limit depending on the circumburst density.

The results of this work highlight the importance of *Chandra* for the determination of short GRB subarcsecond positions, especially in the absence of optical detections. This is critical for locating short GRBs within their host environments, particularly in comparison to *Swift*/XRT position, which are generally much larger than the host galaxy sizes.

R.M. thanks Rodolfo Barniol Duran and Cristiano Guidorzi for useful discussions. We thank Francesco di Mille for carrying out the Magellan FourStar observations, and Andy Monson for assistance with the data reduction. The Berger GRB group at Harvard is supported by the National Science Foundation under grant AST-1107973. Partial support was also provided by NASA/Swift AO6 grant NNX10AI24G. Support for this work was provided by the David and Lucile Packard Foundation Fellowship for Science and Engineering awarded to A.M.S. S.B.C. acknowledges generous financial assistance from Gary & Cynthia Bengier, the Richard & Rhoda Goldman Fund, NASA/Swift grants NNX10AI21G and NNX12AD73G, the TABASGO Foundation, and US National Science Foundation (NSF) grant AST-0908886. A.R. and S.K. acknowledge support by grant DFG Kl 766/16-1. S.S. acknowledges support by a Landesstipendium. Part of the funding for GROND (both hardware and personnel) was generously granted by the Leibniz-Prize to G. Hasinger (DFG grant HA 1850/28-1). Observations were obtained with the JVLA (program 10C-145) operated by the National Radio Astronomy Observatory. The National Radio Astronomy Observatory is a facility of the National Science Foundation operated under cooperative agreement by Associated Universities, Inc. The paper includes data gathered with the 6.5 m Magellan Telescopes located at Las Campanas Observatory, Chile. This work is based in part on observations obtained at the Gemini Observatory, which is operated by the Association of Universities for Research in Astronomy, Inc., under a cooperative agreement with the NSF on behalf of the Gemini partnership: the National Science Foundation (United States), the Science and Technology Facilities Council (United Kingdom), the National Research Council (Canada), CONICYT (Chile), the Australian Research Council (Australia), Ministério da Ciência, Tecnologia e Inovação (Brazil), and Ministerio de Ciencia, Tecnología e Innovación Productiva (Argentina).

REFERENCES

Abazajian, K. N., Adelman-McCarthy, J. K., Agüeros, M. A., et al. 2009, ApJS, 182, 543
Andersen, M. I., de Ugarte Postigo, A., Leloudas, G., & Fynbo, J. P. U. 2011, GRB Coordinates Network, 12563, 1
Barthelmy, S. D., Barbier, L. M., Cummings, J. R., et al. 2005, Space Sci. Rev., 120, 143
Beckwith, S. V. W., Stiavelli, M., Koekemoer, A. M., et al. 2006, AJ, 132, 1729
Belczynski, K., & Kalogera, V. 2001, ApJ, 550, L183
Belczynski, K., Kalogera, V., & Bulik, T. 2002, ApJ, 572, 407
Belczynski, K., Perna, R., Bulik, T., et al. 2006, ApJ, 648, 1110
Berger, E. 2009, ApJ, 690, 231
Berger, E. 2010, ApJ, 722, 1946
Berger, E. 2011, New Astron. Rev., 55, 1
Berger, E., Fong, W., & Sakamoto, T. 2011, GRB Coordinates Network, 12588, 1
Berger, E., Fox, D. B., Price, P. A., et al. 2007, ApJ, 664, 1000
Berger, E., Price, P. A., Cenko, S. B., et al. 2005, Nature, 438, 988
Bernardini, M. G., Margutti, R., Chincarini, G., Guidorzi, C., & Mao, J. 2011, A&A, 526, A27
Bernardini, M. G., Margutti, R., Zaninoni, E., & Chincarini, G. 2012, MNRAS, in press (arXiv:1203.1060)
Bloom, J. S., Kulkarni, S. R., & Djorgovski, S. G. 2002, AJ, 123, 1111
Bloom, J. S., Sigurdsson, S., & Pols, O. R. 1999, MNRAS, 305, 763
Burrows, D. N., Grupe, D., Capalbi, M., et al. 2006, ApJ, 653, 468
Burrows, D. N., Hill, J. E., Nousek, J. A., et al. 2005, Space Sci. Rev., 120, 165
Cenko, S. B., & Cucchiara, A. 2011, GRB Coordinates Network, 12577, 1
Chincarini, G., Mao, J., Margutti, R., et al. 2010, MNRAS, 406, 2113
Dado, S., & Dar, A. 2012, arXiv:1203.5886
de Ugarte Postigo, A., Castro-Tirado, A. J., Guziy, S., et al. 2006, ApJ, 648, L83
Dermer, C. D. 2008, ApJ, 684, 430
Fan, Y.-Z., Wei, D.-M., Zhang, F.-W., & Zhang, B.-B. 2012, arXiv:1204.4881
Foley, S., & Jenke, P. 2011, GRB Coordinates Network, 12573, 1
Fong, W., Berger, E., Chornock, R., et al. 2011a, ApJ, 730, 26
Fong, W., Berger, E., & Fox, D. B. 2010, ApJ, 708, 9
Fong, W., Sanders, N., Milisavljevic, D., & Berger, E. 2011b, GRB Coordinates Network, 12566, 1
Fong, W., Zauderer, B. A., & Berger, E. 2011c, GRB Coordinates Network, 12571, 1
Fong, W.-f., Berger, E., Margutti, R., et al. 2012, arXiv:1204.5475

Fox, D. B., Frail, D. A., Price, P. A., et al. 2005, Nature, 437, 845
Frail, D. A., Kulkarni, S. R., Sari, R., et al. 2001, ApJ, 562, L55
Fryer, C. L., Woosley, S. E., & Hartmann, D. H. 1999, ApJ, 526, 152
Gehrels, N., Chincarini, G., Giommi, P., et al. 2004, ApJ, 611, 1005
Graham, J. F., Fruchter, A. S., Levan, A. J., et al. 2009, ApJ, 698, 1620
Granot, J., & Sari, R. 2002, ApJ, 568, 820
Greiner, J., Bornemann, W., Clemens, C., et al. 2008, PASP, 120, 405
Greisen, E. W. 2003, in Information Handling in Astronomy—Historical Vistas, ed. A. Heck (Astrophysics and Space Science Library, Vol. 285; Dordrecht: Kluwer), 109
Grupe, D., Burrows, D. N., Patel, S. K., et al. 2006, ApJ, 653, 462
Hill, J., Burrows, D. N., Nousek, J. A., et al. 2004, Proc. SPIE, 5165, 217
Hjorth, J., Watson, D., Fynbo, J. P. U., et al. 2005, Nature, 437, 859
Hogg, D. W., Pahre, M. A., McCarthy, J. K., et al. 1997, MNRAS, 288, 404
Hook, I. M., Jørgensen, I., Allington-Smith, J. R., et al. 2004, PASP, 116, 425
Ioka, K., Kobayashi, S., & Zhang, B. 2005, ApJ, 631, 429
Kalberla, P. M. W., Burton, W. B., Hartmann, D., et al. 2005, A&A, 440, 775
Kaneko, Y., Preece, R. D., Briggs, M. S., et al. 2006, ApJS, 166, 298
Kennicutt, R. C., Jr. 1998, ARA&A, 36, 189
Lazzati, D., Blackwell, C. H., Morsony, B. J., & Begelman, M. C. 2011, MNRAS, 411, L16
Leibler, C. N., & Berger, E. 2010, ApJ, 725, 1202
Levan, A. J., Tanvir, N. R., Fruchter, A. S., et al. 2006a, ApJ, 648, L9
Levan, A. J., Wynn, G. A., Chapman, R., et al. 2006b, MNRAS, 368, L1
Mangano, V., Baumgartner, W. H., Beardmore, A. P., et al. 2011a, GRB Coordinates Network, 12559, 1
Mangano, V., Baumgartner, W. H., Krimm, H. A., et al. 2011b, GCN Rep. 363
Maraston, C. 2005, MNRAS, 362, 799
Margutti, R., Chincarini, G., Granot, J., et al. 2011, MNRAS, 417, 2144
Margutti, R., Zaninoni, E., Bernardini, M. G., et al. 2012, arXiv:1203.1059
Melandri, A., Fugazza, D., Covino, S., & Palazzi, E. 2011a, GRB Coordinates Network, 12570, 1
Melandri, A., Sbarufatti, B., Stratta, G., et al. 2011b, GRB Coordinates Network, 12565, 1
Metzger, B. D., Quataert, E., & Thompson, T. A. 2008, MNRAS, 385, 1455
Oates, S. R., & Mangano, V. 2011, GRB Coordinates Network, 12569, 1
Perley, D. A., Metzger, B. D., Granot, J., et al. 2009, ApJ, 696, 1871
Perley, R. A., Chandler, C. J., Butler, B. J., & Wrobel, J. M. 2011, ApJ, 739, L1
Perna, R., & Belczynski, K. 2002, ApJ, 570, 252
Predehl, P., & Schmitt, J. H. M. M. 1995, A&A, 293, 889
Roming, P. W. A., Kennedy, T. E., Mason, K. O., et al. 2005, Space Sci. Rev., 120, 95
Sakamoto, T., Barthelmy, S. D., Baumgartner, W. H., et al. 2011a, GRB Coordinates Network, 12561, 1
Sakamoto, T., Troja, E., Gehrels, N., et al. 2011b, GRB Coordinates Network, 12580, 1
Sakamoto, T., Troja, E., Aoki, K., et al. 2012, arXiv:1205.6774
Schlafly, E. F., & Finkbeiner, D. P. 2011, ApJ, 737, 103
Schmidl, S., Rossi, A., Kann, D. A., & Greiner, J. 2011, GRB Coordinates Network, 12568, 1
Soderberg, A. M., Berger, E., Kasliwal, M., et al. 2006, ApJ, 650, 261
Willmer, C. N. A., Faber, S. M., Koo, D. C., et al. 2006, ApJ, 647, 853
Zhang, B., Fan, Y. Z., Dyks, J., et al. 2006, ApJ, 642, 354
Zhao, X.-H., Xu, D., Mao, J.-R., & Bai, J.-M. 2011, GRB Coordinates Network, 12560, 1